ISSN 2075-1087, Gyroscopy and Navigation, 2024, Vol. 15, No.1, pp. 52-60
Russian Text © The Author(s), 2024, published in Giroskopiya i Navigatsiya, 2024, No. 1, pp. 72-83

Detection of a Dipole Signal against the Background of Noise under Arbitrary Motion of the Magnetometer Carrier

G.V. Antsev[a], V.V. Averkiev[a]*, V.A. Mogilevkin[a], and I.A. Chernyaev[a]

[a]*JSC Radar mms, St. Petersburg, Russia*
**e-mail: averkiev_vv@radar-mms.com*
Received February 7, 2024; reviewed April 6, 2024; accepted April 10, 2024

Abstract: The article describes an algorithm for detecting a dipole signal against the background of noise under arbitrary motion of the magnetometer carrier. The constructed dipole mathematical model in the form of expansion in a series of six basis functions provides source recognition and estimation of the source position from the single detection. The hardware-in-the-loop simulation results are presented.

Keywords: dipole source, expansion into a series of basis functions, arbitrary motion of the magnetometer carrier, estimation of source coordinates.

1. INTRODUCTION

Autonomous navigation aids for aircraft and maritime carriers are being intensively developed. Inertial navigation systems (INS), which are widely applied, satisfy most of the requirements, with the exception of the duration of autonomous navigation.

The accuracy of autonomous navigation can be enhanced by INS aiding with a system using additional sources of positioning data, such as a global satellite navigation system (GNSS).

The idea of using the Earth's magnetic field (EMF) for this purpose appeared quite a long time ago [1, 2, 3, 4]. The principal operability of the navigation system with INS EMF aiding was confirmed experimentally [2, 12, 13, 14, 15]. The geomagnetic field is a perspective additional source of navigation information due to its global nature, stability, and noise immunity. EMF-based INS aiding systems are particularly demanded in oversea flights or in navigation, including underwater, when other additional autonomous positioning aids may be not available (optical contrast navigation, terrain-aided navigation, etc.).

The anomalous EMF (AEMF) is the most informative in the carrier positioning, since it contains spatially high-frequency components unlike the main magnetic field.

In geomagnetic navigation technologies, it is necessary to distinguish the AEMF parameters, for which the maps exist. We also need the sensors installed on moving carriers. The parameters of the AEMF include:

- AEMF magnitude;
- AEMF vector;
- AEMF gradient.

The AEMF magnitude is obviously the first candidate due to the presence of maps and quantum magnetometers providing the highest measurement accuracy. Methods for compensating the carrier magnetic interference have been well developed, which is important for installing the magnetometer on board the carrier.

Recently, global magnetic field maps of various Earth regions have appeared [9, 17, 18, 19] that can be potentially used for continuous INS aiding. The magnetic field variations constrain the accuracy of magnetic field-aided navigation. At the same time, the AEMF is unstable and relatively slowly changes with time [10], which requires periodic updating of existing maps.

Using the AEMF vector as an informative parameter potentially provides higher navigation accuracy. The navigation system using AEMF vector aiding can be built based on the global spatial digital model of AEMF components developed at Pushkov Institute of Terrestrial Magnetism, Ionosphere and Radio Wave Propagation of the Russian Academy of Sciences (IZMIRAN) [20, 21, 22]. The model allows

constructing the field vector maps based on its magnitude for a certain geographic area. The disadvantages include the need to accurately determine the carrier attitude to calculate the EAMF components in inertial space and the fact that the available vector magnetometers are at least order of magnitude less accurate than scalar ones.

As to maritime vehicles, a navigation system with AEMF gradient aiding is preferable. It is robust to EMF variations, and the AEMF gradient is more stable over time compared to the field magnitude. The difficulty in using this system, similarly to the system using the field vector as an informative parameter, is the need to determine the carrier attitude with high accuracy (here, to obtain the EMF gradient in inertial space). Installing several magnetometers on board the carrier is an additional challenge.

This paper studies an INS aiding system with detection of AEMF characteristic dipole sources in the form of short length dipole anomalies. Determining the coordinates of the detected sources and comparing them with the map makes it possible to correct the INS errors at certain points.

The system includes an INS, a high-sensitivity quantum magnetometer aided by a three-component magnetometer to compensate for carrier magnetic interference, and a digital EMF anomaly map. The INS vehicle coordinates over its motion interval are converted into EMF anomalies using a digital map, which are compared with the anomalies detected by the quantum magnetometer and cleared of noise.

2. MODEL OF THE DIPOLE USEFUL SIGNAL

Physical bodies, both man-made or natural, having a magnetic moment can be described with a model of a magnetic dipole or a set of dipoles. In the reference frame bound with the rectilinear motion of the magnetometer carrier, the magnetic field of the dipole can be represented as

$$\Delta T_c(\mathbf{r}(t)) \approx \approx \frac{\mu_0}{4\pi R(t)^5} \cdot \mathbf{b}^T \cdot \begin{bmatrix} 3r_x^2(t) - R^2(t) & 3r_x(t) r_y & 3r_x(t) r_z \\ 3r_y r_x(t) & 3r_y^2 - R^2(t) & 3r_y r_z \\ 3r_z r_x(t) & 3r_z r_y & 3r_z^2 - R^2(t) \end{bmatrix} \cdot \mathbf{M}, \quad (1)$$

where **M** is the vector of the dipole magnetic moment in the accepted frame; **b** is the unit vector of the EMF in the accepted frame; r_x is the magnetometer position on the route relative to the dipole; r_y, r_z are the lateral and vertical displacements of the magnetometer relative to the dipole, respectively; $R(t) = \sqrt{r_x^2(t) + r_y^2 + r_z^2}$ is the current distance to the dipole.

These bodies against the background of the main Earth's magnetic field are the brightness marks tied to coordinates. The marks detected by an onboard magnetometer are matched with the reference EMF map to serve as reference points for INS aiding.

The traditional algorithm for dipole signal detection against the noise background used in modern magnetic detectors is based on representing the dipole signal in the form of an expansion into an orthonormal series consisting of three basis functions [6]. These functions depend on the traverse distance to the dipole and the carrier speed. The expansion is true for the carrier rectilinear motion relative to the signal source. The processing system therefore becomes multi-channel with respect to one coordinate – motion along the route.

The experience in operating the airborne magnetometers shows that this limitation is extremely inconvenient for the following reasons:

• the dipole detection algorithm fails to determine the source coordinates from a single contact, since it is unknown whether it is located to the right or left of the motion trajectory;

• the decision making time increases, because the carrier should fly a straight distance after the traverse equal to two to three ranges for which the processing channel is configured;

• trajectory deviation from a straight line leads to enhanced noise associated with the EMF gradient.

To remove these shortcomings, the authors have performed a generalized expansion of the dipole signal into a series of basis functions of the carrier arbitrary motion in the horizontal plane. Based on the expansion, we have developed an algorithm for anomaly detection – a two-coordinate detector, which determines the coordinates of the detected dipole from the single contact, compares them with the EMF map, and corrects INS errors.

3. UNIVERSAL DIPOLE SIGNAL DETECTION ALGORITHM

The dipole signal model can be represented as follows. The magnetic induction vector of the dipole field $B_D(t)$ is added to the magnetic induction vector

of EMF. An absolute magnetometer produces the signal being the difference between the magnitudes of the vectors of the specified sum and the EMF magnetic induction. The object field is extremely small as compared to the EMF, therefore, the signal can be recorded as a projection

$$s(t)=\mathbf{b}^T\mathbf{B}_D(t), \quad (2)$$

where **b** is the unit vector of EMF magnetic induction in the accepted reference frame, $\mathbf{b}^T$ is the row vector.

Considering the general formula for the dipole magnetic field (1), $s(t)$ is reduced to

$$s(t)=\frac{\mu_0}{4\pi R^5(t)}\mathbf{b}^T\left[3\mathbf{R}(t)\mathbf{R}^T(t)-R^2(t)\mathbf{E}\right]\mathbf{M}, \quad (3)$$

where **R** is the radius vector of the magnetometer position relative to the object in the selected frame; **M** is the object magnetic moment vector in this frame; **E** is the identity matrix.

To specify the signal model in a two-dimensional plane, we should determine the working frame.

Assuming that the magnetometer carrier is moving at a constant height (Dz is constant), we will only mind the direction of the horizontal axes. Consider a frame with an origin at the fixed point W_0 of the detection window and the axis Ωξ codirectional with the velocity vector **v** at this point (Fig. 1).

The coordinates of an arbitrary point W_c on the trajectory *TP* in Ωξη frame with respect to the local navigation North-East-Down frame *Oxy* are determined as

$$\begin{aligned}\xi_c&=\left(r_{x_c}-r_{x_0}\right)\cos\varphi+\left(r_{y_c}-r_{y_0}\right)\sin\varphi,\\ \eta_c&=-\left(r_{x_c}-r_{x_0}\right)\sin\varphi+\left(r_{y_c}-r_{y_0}\right)\cos\varphi,\end{aligned} \quad (4)$$

where φ is the course over ground.

The frame Ωξη is referred to as the velocity frame. Its horizontal axes change their directions with the horizontal velocity vector, which is typical for a curvilinear trajectory.

When the axis Ωξ is codirectional with the course over ground at point W_0, it is the traverse point that can be made the frame origin, that is,

$$\xi_c(t_0)=\eta_c(t_0)=0. \quad (5)$$

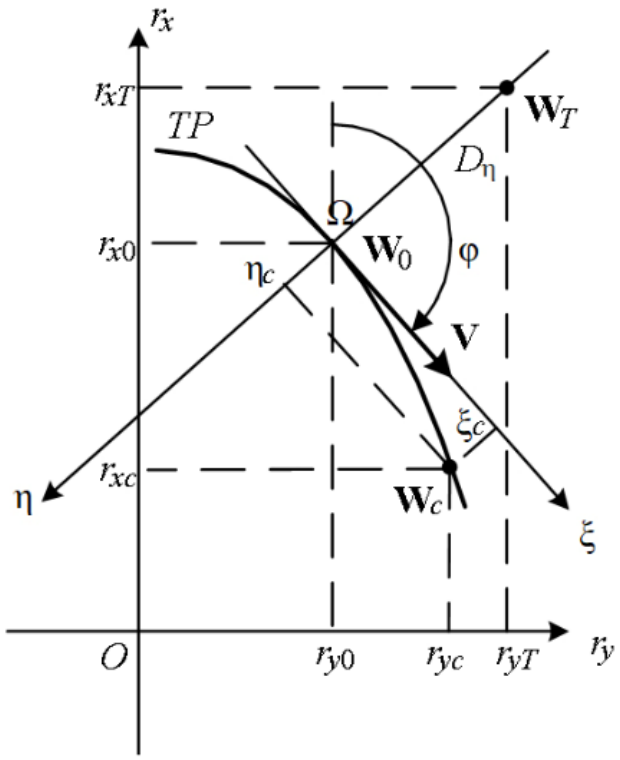

Fig. 1. Two Cartesian frames: *Oxy* and Ωξη

According to Fig. 1, at time t_0 the target coordinates ξ_T and η_T take the values

$$\xi_T(t_0)=0,\ \eta_T(t_0)=-D_\eta. \quad (6)$$

The vertical distance to the target is denoted with D_Z, then the traverse distance will be $D=\sqrt{D_\eta^2+D_Z^2}$.

Assume that the object velocity can be neglected unlike the magnetometer carrier velocity, then the distance to the dipole $R(t)$ can be presented as

$$R(t)=D\sqrt{1+\frac{\left[\xi_c(t)\right]^2+\left[\eta_c(t)\right]^2-2D_\eta\eta_c(t)}{D^2}}. \quad (7)$$

The distance to the dipole parametrically depends not only on time, but also on the point taken to be t_0: $R = R(t, t_0)$. To simplify the further formulas, we omit the explicit $R - t_0$ dependence.

Using the normalized variables

$$\begin{aligned}d_\eta&=\frac{D_\eta}{D},\\ d_z&=\frac{D_z}{D},\\ \bar{\xi}_c(t)&=\frac{1}{D}\xi_c(t),\\ \bar{\eta}_c(t)&=\frac{1}{D}\eta_c(t),\end{aligned}$$

we write the normalized distance to the dipole as

$$\bar{R}(t)=\frac{R(t)}{D}=\sqrt{1+\left[\bar{\xi}_c(t)\right]^2+\left[\bar{\eta}_c(t)\right]^2-2d_\eta\bar{\eta}_c(t)}. \quad (8)$$

Using the model (3) and making the algebraic transformations, we obtain the following sought expansion of the object signal s for an arbitrary carrier trajectory in the horizontal plane:

$$\begin{aligned} &s\left(\bar{\xi}_c(t),\bar{\eta}_c(t),D,d_\eta\right)= \\ &=\mu_0/4\pi D^3\sum_{i=1}^{6}\alpha_i\Psi_i\left(\bar{\xi}_c(t),\bar{\eta}_c(t),d_\eta\right). \end{aligned} \quad (9)$$

The basis functions of the signal Ψ_i are given by

$$\begin{aligned} &\Psi_1(t)=1/\bar{R}^5(t), \\ &\Psi_2(t)=\bar{\xi}_c(t)/\bar{R}^5(t), \\ &\Psi_3(t)=\bar{\eta}_c(t)/\bar{R}^5(t), \\ &\Psi_4(t)=\bar{\xi}_c(t)\bar{\eta}_c(t)/\bar{R}^5(t), \\ &\Psi_5(t)=\left[\bar{\eta}_c(t)\right]^2/\bar{R}^5(t), \\ &\Psi_6(t)=\left[\bar{\xi}_c(t)\right]^2/\bar{R}^5(t) \end{aligned} \quad (10)$$

and are completely determined by the carrier motion with respect to the dipole source.

It is important to note that expansion (9) is accurate, that is, it describes the dipole signal without methodological errors. In accordance with this concept, the useful signal is determined accurate to the dipole position parameters D, d_η at unknown time t_0 and coefficients α_i. It can be shown that the expansion coefficients depend on the unit vector of the EMF inductance vector **b** and the dipole magnetic moment vector **M**.

The number of independent expansion terms (basis functions) is varying depending on the type of motion. In the case of rectilinear motion, the lateral coordinate $\eta_c(t)$ becomes zero, and expansion (9) contains only three basis functions – $\Psi_1(t)$, $\Psi_2(t)$, $\Psi_6(t)$, which yields the known representation of the dipole signal (1). Here, data on the dipole lateral position d_η is lost, that is, during rectilinear motion it is not known whether the dipole is located to the right or left of the carrier. In the case of circular motion (with constant curvature), five basis functions $\Psi_1(t)$, $\Psi_2(t)$, $\Psi_3(t)$, $\Psi_4(t)$, $\Psi_6(t)$ are independent.

From the fact that at least five basis functions are linearly independent during curvilinear motion of the carrier, it follows that the traverse distance D and lateral displacement D_η can be found. Adding the carrier position at the traverse time t_0, we obtain all three coordinates of the dipole position. Thus, the dipole position is determined within one pass with a single magnetic detector. From the explicit form of the basis functions of the signal expansion, a linearly independent basis for an arbitrary realized horizontal motion of the magnetometer can be determined, and thereby decided whether dipole positioning is possible in each case. This distinguishes the proposed expansion from the standard representation of a dipole signal, in which the distance to the dipole is represented as a two-dimensional grid [23].

We substitute the obtained object coordinates to (3) and solve a linear system of equations for the components M_x, M_y, and M_z of the vector **M**, then we calculate the magnetic moment of the search object, that is, classify it.

The search for an object is performed in conditions of interference caused by various factors. This means that relevant appropriate interference models are required for the detector operation. It should be borne in mind that these models describe the components of interference on a sliding interval, that is, in the detection window.

The field of the search object is observed against the background of EMF anomalies, which impede the detection to the extent that their spectra intersect. On the one hand, the power of the spectrum of the EMF profile significantly exceeds the power of the object anomaly (usually by several orders of magnitude). On the other hand, it is concentrated in the low frequency domain and its decrease rate grows with the anomaly depth. Hence, a dipole source can be detected only if the traverse distance to it is much less than to the nearest EMF anomalies. Then the spectrum of the sought object will shift relative to the EMF spectrum to the high frequency domain.

The EMF profile is modeled in the wind frame (Fig. 1) as follows. First, we determine the course over ground $\bar{\bar{\varphi}}$ at the supposed traverse point $\mathbf{r}_0$ from the aircraft coordinates **r** in the detection window $[t-\tau, t]$, which are assumed to be known. Then, using transformation (6), we calculate the displacement vector in the wind frame on the detection interval.

Generally the EMF in the search area is unknown, it can only be stated to be infinitely differentiable as a potential field, so its profile in the detection window $[t-\tau, t]$ is described as

$$T\left(\xi_c(t),\eta_c(t),r_z(t)\right)\cong$$
$$\cong T\left(\xi_c(t)\right)+\frac{\partial T}{\partial \eta}\left(\xi_c(t)\right)\eta_c(t)+\frac{\partial T}{\partial z}\left(\xi_c(t)\right)\delta r_z(t), \quad (11)$$

based on the field gradient. This representation considers the vertical deviations of the real motion from the medium r_{z_0} on the detection interval:

$$\delta r_z(t)=r_z(t)-r_{z_0}.$$

The components of the gradient $\frac{\partial T}{\partial \eta},\frac{\partial T}{\partial z}$ are the functions of the longitudinal displacement $\xi_c(t)$. The functions $T\left(\xi_c\right),\frac{\partial T}{\partial \eta}\left(\xi_c\right),\frac{\partial T}{\partial z}\left(\xi_c\right)$ can be approximated with the polynomials of different degrees. These degrees can be rationally selected based on a priori data on the sea depth or, which is better, on EMF of the search area (using, for example, the model EMAG2 [10]).

Detection can also be limited by the error in carrier interference compensation. This is due to several reasons. First, if the initial interference is large, the compensation error, proportional to the second order of smallness of the variation in attitude angles, also turns out to be high. Second, the interference model assumes the constant magnetic fields created by the aircraft, which is not always true, for example, after repair or replacement of some parts. Moreover, there is a non-stationary residual interference, which is caused by currents in the aircraft electrical circuits.

The carrier residual interference is estimated with a model functionally depending on aircraft attitude relative to the EMF measured in increments of the EMF components $\mathbf{B}_x$, $\mathbf{B}_y$ relative to their average value on the detection interval. The carrier residual interference model is optional, meaning that its use depends on how electromagnetic compatibility requirements are met in magnetometer installation on board the carrier.

In general, the model of the field magnitude T in the detection window is represented as an expansion

$$T\left(t,\xi_c,\eta_c,r_z,\mathbf{B}_x,\mathbf{B}_y\right)=\sum_{i=1}^{M}\beta_i\Phi_i\left(\xi_c,\eta_c,r_z,\mathbf{B}_x,\mathbf{B}_y\right) \quad (12)$$

with the known functions Φ_i depending on the carrier position in the wind frame (ξ_c, η_c, r_z) and EMF components $\mathbf{B}_x$, $\mathbf{B}_y$. The expansion coefficients for β_i are not determined.

Form the basis functions of the interference Φ_i and signal Ψ_i using the navigation data $\xi_c^*(t),\eta_c^*(t),r_Z^*(t)$ and three-component magnetometer data $\mathbf{B}_x^*,\mathbf{B}_y^*$.

The models (12) and (9) contain unknown parameters that can take many values. When constructing the decision rules for the processing algorithms, a priori uncertainty can be resolved using an approach, where unknown parameters are estimated for both hypotheses used in the likelihood ratio as if they were true [10]. We set a two-dimensional grid with the coordinates being the distance and lateral deviation $\{D_k, D_{\eta l}\}$ and estimate the linearly inputted parameters $\{\alpha_i, \beta_i\}$ to obtain an object detection algorithm similar to that described in [6, 7, 11]. The difference is that one-dimensional signal and interference models are generalized to the case of arbitrary motion in the horizontal plane.

4. DIPOLE SIGNAL DETECTION ALGORITHM

The detection algorithm was simulated during the curvilinear motion using the data from MMS-27 magnetometer in real flight on board Ka-27M helicopter.

The block diagram of the detection algorithm is shown in Fig. 2.

The search based on integrated processing of magnetometric and navigation data is performed continuously independent of the flight trajectory, and the dipole signal can be detected at any portion, including the turns.

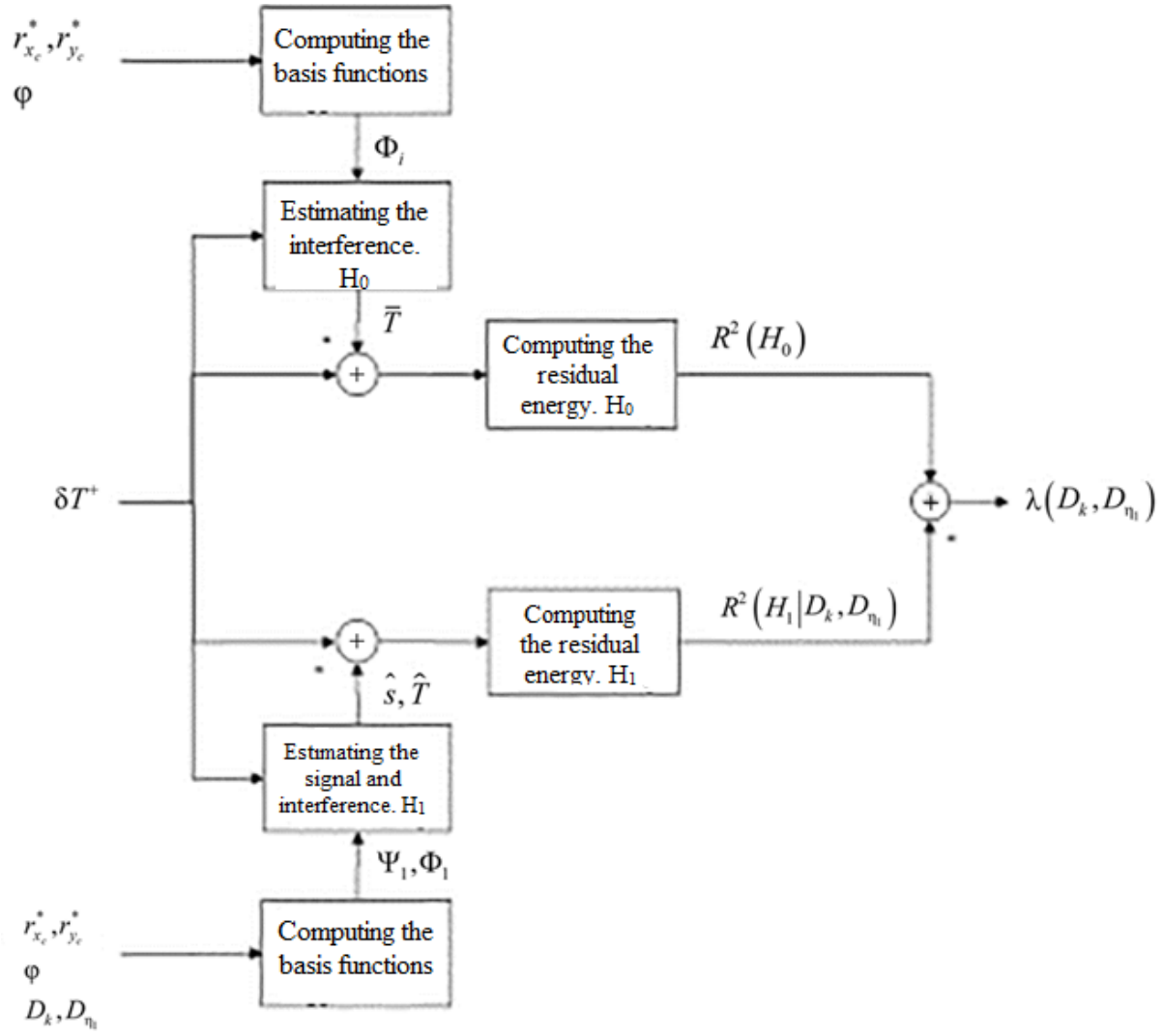

Fig. 2. Block diagram of the detection algorithm.

5. RESULTS FROM HARDWARE-IN-THE-LOOP SIMULATION

The detection algorithm has been simulated on a rectilinear route (Fig. 3a) and during the turn (Fig. 3b). It should be noted that consideration for the real helicopter motion reduces the detection of false targets due to the geomagnetic field gradient on rectilinear routes. The improvement in signal-to-noise ratio in the case of using the two-dimensional signal description is also noted in [23], however, it does not imply dipole localization.

The output signal of the magnetometer detector is shown in Fig. 4. The data were obtained with MMS-27S magnetometer installed on board the IL-114LL research airplane during the flight over the dam in the Gulf of Finland.

The coordinates were determined while passing between the shutters of the dam gates. The dam magnetic field is a spatial structure consisting of many dipoles, so the magnetometer at an altitude of 300 m perceives the total field. The device actually detected the magnetic center of the object on the water surface, which is probably due to the dam symmetrical design.

The radar system was installed on board the aircraft to aid the positioning of the dam passage. The radar system determines the passage coordinates using a radar image with a 10 m resolution.

The points where the coordinates were obtained using the radar and magnetometer data are shown in Fig. 5.

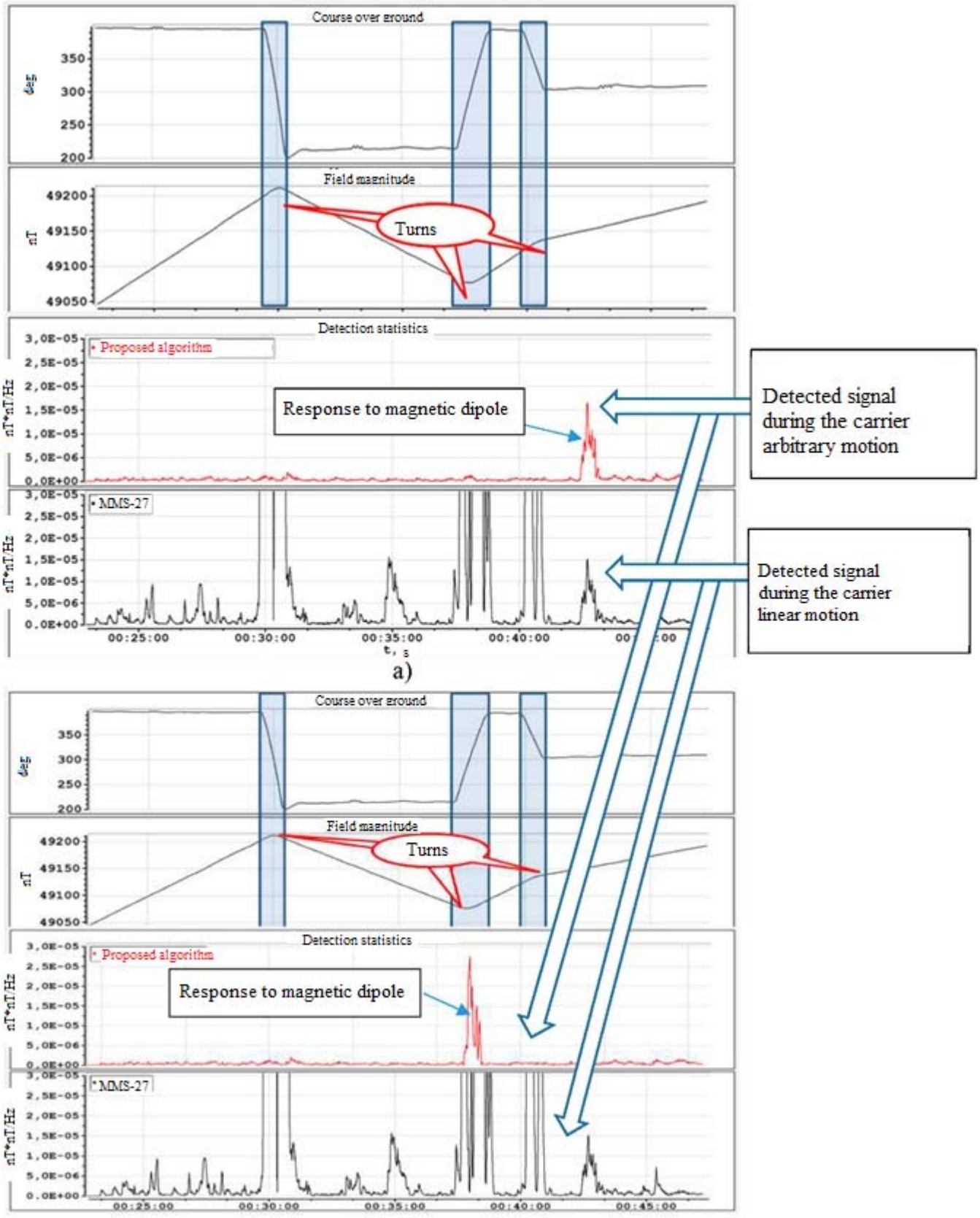

Fig. 3. Simulation of dipole signal detection algorithm: a – on rectilinear route, b – during the turn.

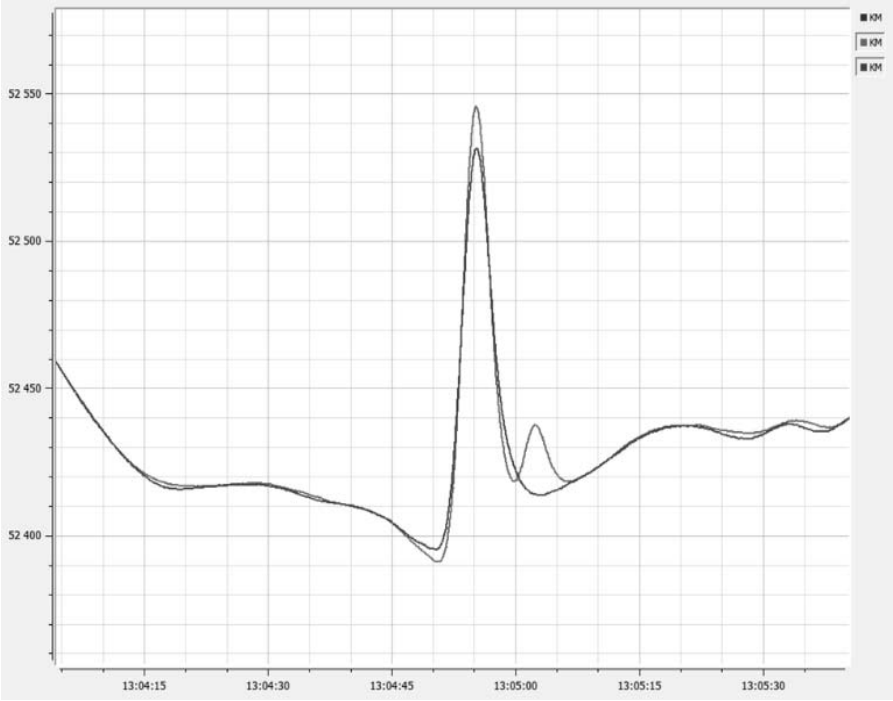

Fig. 4. Magnetometer output signal. One curve is the first flight over the dam, the second curve in the return flight.

Fig. 5. Flight path over the dam with the points showing the radar and magnetometer detections.

6. CONCLUSIONS

The proposed mathematical model of the dipole signal during arbitrary motion of the magnetometer carrier provides the design of an optimal multi-channel spatial detector. It reduces the number of false targets due to the carrier motion in the geomagnetic field gradient and estimates the dipole coordinates in one pass. Matching the obtained dipole coordinates with the geomagnetic field map enhances the noise immunity of navigation systems if no GNSS data are available.

FUNDING

This work was supported by ongoing institutional funding. No additional grants to carry out or direct this particular research were obtained.

CONFLICT OF INTEREST

The authors of this work declare that they have no conflicts of interest.

REFERENCES

1. Krasovskii, A.A., Beloglazov, I.N., and Chigin, G.P., *Teoriya korrelyatsionno-ekstremal'nykh navigatsionnykh system* (Theory of Correlation-Extreme Navigation Systems), Moscow: Nauka, 1979.
2. Beloglazov, I.N., Dzhandzhgava, G.I., and Chigin, G.P., *Osnovy navigatsii po geofizicheskim polyam* (Fundamentals of Map-Aided Navigation), Moscow: Nauka, 1985.
3. Dzhandzhgava, G.I., Gerasimov, G.I., and Avgustov, L.I., Map-aided navigation and guidance, *Izvestiya YuFU. Tekhnicheskie nauki*, 2013, no. 3, pp. 74–84.
4. https://www.ngdc.noaa.gov/geomag/emag2.html.
5. Karshakov, E.V., Using the measurements of the Earth's magnetic field gradient in aircraft navigation, *Upravlenie bol'shimi sistemami*, 2011, no. 35.
6. Semevskii, R.B., Averkiev, V.V., and Yarotskii, V.A., *Spetsial'naya magnitometriya* (Special Magnetometry), St. Petersburg: Nauka, 2002.

7. Averkiev, V.V. and Petukhov, Yu. M., Optimization of the search for local magnetic anomalies using a magnetic detector, *Measurement Techniques*, 2013, vol. 55, no. 12, pp. 1413–1416. https://doi.org/10.1007/s11018-013-0142-0
8. Antsev, I.G., Averkiev, V.V., and Petukhov, Yu. M., A nonlinear compensator of the magnetic interference of an aviation magnetometer system, *Measurement Techniques,* 2014, vol. 57, no. 3, pp. 347–352. https://doi.org/10.1007/s11018-014-0458-4
9. Antsev, I.G., Averkiev, V.V., and Petukhov, Yu. M., A nonlinear compensator of the magnetic interference of an aviation magnetometer system. Algorithm ANN-2, *Measurement Techniques,* 2015, vol. 58, no.3. https://doi.org/10.1007/s11018-015-0710-6
10. Meyer, B., Chulliat, A., and Saltus, R., Derivation and error analysis of the Earth Magnetic Anomaly Grid at 2 arc min resolution Version 3 (EMAG2v3), *Geochemistry, Geophysics, Geosystems*, 2017, vol. 18, no. 12, pp. 4522–4537. https://doi.org/10.1002/2017GC007280
11. Van Trees, H.L., *Detection, Estimation, and Modulation Theory*, Part 1, *Detection, Estimation, and Linear Modulation Theory*, John Wiley and Sons, 1968.
12. Baklitskii, V.K., *Korrelyatsionno-ekstremal'nye metody navigatsii i navedeniya* (Correlation Extreme Navigation and Guidance Methods), Tver: Knizhnyi Klub, 2009.
13. Beloglazov, I.N., and Tarasenko, V.P., *Korrelyatsionno-ekstremal'nye systemy* (Correlation-Extreme Systems), Moscow: Radio, 1974.
14. Volkovitskii, A.K., Karshakov, E.V., and Pavlov, B.V., *Magnitogradientnye izmeritel'nye sistemy i kompleksy* (Magnetic Gradient Measurement Systems and Complexes), in 2 vols., Moscow: Trapeznikov Institute of Control Sciences, 2018.
15. Volkovitsky, A.K., Karshakov, E.V., Moilanen, E.V., and Pavlov, B.V., Integration of magnetic gradiometer correlation-extremal and inertial navigation systems, *19th St. Petersburg International Conference on Integrated Navigation Systems*, 2012.
16. Akimov, P.S., Bakut, P.A., Bogdanovich, V.A. et al., *Teoriya obnaruzheniya signalov* (Signal Detection Theory), Moscow: Radio i svyaz', 1984.
17. Bickel, S.H., Small signal compensation of magnetic fields resulting from aircraft maneuvers, *IEEE Trans. v. AES-15*, 1979, no. 4.
18. Khvostov, O.P., Theory of splitting the magnetic interference of the magnetometer carrier, *Geofizicheskoe priborostroenie*, 1962, no. 14.
19. Leach, B.W., Aeromagnetic compensation as a linear regression problem, *Information Linkage between Applied Mathematics and Industry*, Academic Press, 1980, pp. 139–161.
20. Kopytenko, Yu.A., Petrova, A.A., and Avgustov, L.I., Analysis of informativeness of the Earth's magnetic field for autonomous correlation-extreme navigation, *Fundamental'naya i prikladnaya geofizika*, 2017, vol. 10, no. 1.
21. Kopytenko, Yu.A. and Petrova, A.A., New generation magnetic maps for maritime magnetic navigation, Proceedings of the 12th Russian Conference *Prikladnye tekhnologii gidroakustiki i gidrofiziki* (Applied Hydroacoustic and Hydrophysics Technologies), St. Petersburg: Nestor-Istoriya, 2014.
22. Kopytenko, Yu.A. and Petrova, A.A., Results from development and application of the component Earth's magnetic field model in magnetic cartography and geophysics, *Fundamental'naya i prikladnaya geofizika,* 2016, vol. 9, no. 2, pp. 88—106.
23. Xingen Liu, Zifan Yuan, Changping Du, Xiang Peng, Hong Guo, and Mingyao Xia, Adaptive basis function method for the detection of an undersurface magnetic anomaly target, *Remote Sensing*, 2024, vol. 16, 363. https://doi.org/10.3390/rs16020363